A Finite Control Set Model Predictive Control for Five-Phase PMSMs With Improved DC-Link Utilization

Bin Yu, *Student Member, IEEE*, Wensheng Song, *Member, IEEE*, Yongqi Guo, and Mahmoud S. R. Saeed

***Abstract*—Finite control set model predictive control (FCS-MPC) based on virtual voltage vectors (V3s) is widely studied and applied in five-phase permanent magnet synchronous motor (PMSM) drives. The synthesized V3s can inherently eliminate *xy*-axes voltages and reduce the number of candidate vectors, which can significantly reduce the computation burden. However, the dc-link utilization is reduced due to the usage of V3s. To address this issue, an FCS-MPC method with improved dc-link utilization is proposed in this article. First, only large vectors are selected to predict the system evolution. The large vector that minimizes cost function is selected, and rescaled using the duty ratio estimation. Then, in order to control the third harmonic currents, three adjacent large vectors are applied to replace the selected vector, and the duty ratios are reassigned. Additionally, zero vectors are replaced with two opposite large vectors to reduce common-mode voltage (CMV). Finally, the proposed FCS-MPC is compared with conventional methods in experiments. Experimental results have verified that the proposed method can improve the dc-link utilization, and keep the superiorities of low CMV and low computation burden.**

***Index Terms*—Common-mode voltage (CMV), dc-link utilization, finite control set model predictive control (FCS-MPC), five-phase drives, permanent magnet synchronous motor (PMSM).**

I. Introduction

MULTIPHASE permanent magnet synchronous motor (PMSM) drives have attracted much attention in the recent years due to their attractive features [1]–[3]. Compared with the three-phase counterparts, multiphase PMSM drives offer enhanced fault-tolerant capability, reduced current stress per phase, low torque ripples and high torque density [4]–[6].

Improving the dc-link utilization in multiphase drives brings several benefits [7], [8]. For a given motor, high dc-link utilization allows decreasing the dc-link voltage, which facilitates complying with voltage limitations imposed by other components and isolation requirements. For a given dc-link voltage, high dc-link utilization means high stator voltage, which can extend the speed range [9]. Hence, dc-link utilization improvement is one of the research hotspots in multiphase drives [10]–[15]. To fully utilize the dc-link volage, space vector pulsewidth modulation methods have been proposed for five-phase drives [10], [11] and dual three-phase drives [12]. Carrier-based pulsewidth modulation methods with high dc-link utilization are also proposed for five-phase drives [13], [14], and extended to symmetrical and asymmetrical multiphase drives [15]. However, there are rarely few studies investigating the dc-link utilization of model predictive control for five-phase PMSM drives.

Finite control set model predictive control (FCS-MPC) is becoming a promising control method in electrical drives, due to the characteristics of fast dynamic performance, intuitive principle and easy handling of nonlinear constraints [16], [17]. FCS-MPCs take advantage of the discrete natures and finite switching states of inverters to solve the optimization problem. All available vectors are used to estimate the system evolution during each sampling interval, the one that minimizes the predefined cost function is selected and applied in the next interval. Therefore, FCS-MPC for multiphase drives suffers from heavy computation burden [18]. The idea of virtual voltage vector (V3) is a popular solution to reduce the computation burden and improve steady-state performance of FCS-MPC in multiphase applications [19]–[21]. The synthesized V3s can cancel the *xy*-axes voltages in five-phase [22] and six-phase drives [23], and the third harmonic currents are inherently eliminated. Moreover, the number of V3s is significantly reduced, which can simplify the computation burden. However, since the amplitude of synthesized V3s is lower than large vectors, the dc-link utilization is reduced in this kind of V3-based FCS-MPC methods [24].

Common-mode voltage (CMV) is another issue that should be concerned in multiphase PMSM drives. CMV is known to cause bearing currents, which will damage the motor bearings [25], [26]. There are three different components in the bearing currents [27]: *dv*/*dt* bearing current stemming from step changes in the CMV; electrical discharge machining (EDM) current; and circulating bearing current along the motor shaft and frame through two bearings. Among the different types of bearing currents, the EDM current is the highest, which results from the dielectric breakdown of the lubricant caused by the shaft peak voltage. On the other hand, a percentage of CMV (typically 10%) appears as the shaft voltage [28], [29]. Therefore, it is reasonable

Manuscript received April 14, 2021; revised August 1, 2021; accepted September 5, 2021. Date of publication September 16, 2021; date of current version November 30, 2021. This work was supported by the National Natural Science Foundation of China under Grants 52022084 and U1934204. Recommended for publication by Associate Editor R. Kennel. (*Corresponding author: Wensheng Song*.)

The authors are with the School of Electrical Engineering, Southwest Jiaotong University, Chengdu 610031, China (e-mail: yubin_electric@163.com; songwsh@swjtu.edu.cn; yq_guo_swjtu@163.com; mahmoud.said@eng.svu.edu.eg).

Color versions of one or more figures in this article are available at https://doi.org/10.1109/TPEL.2021.3113032.

Digital Object Identifier 10.1109/TPEL.2021.3113032

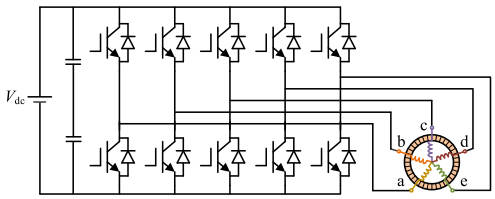

Fig. 1. Topology of a five-phase PMSM fed by a two-level VSI.

to reduce CMV, which in turn prevents the destructive bearing currents.

In this article, an FCS-MPC method with improved dc-link utilization is proposed for five-phase PMSM drives. First, the ten large vectors are used to predict the currents evolution and evaluate the cost function. The third harmonic terms are cancelled from the cost function, and the large vector that minimizes the simplified cost function is selected. The duty ratio of the selected vector is also estimated and limited within $0 \leq d \leq 1$, which can reduce the current tracking errors. Then, three adjacent large vectors are selected to replace the optimal vector, and the duty ratios are reassigned, without breaking the volt-second balance in $\alpha\beta$ subspace. In linear modulation region ($0 \leq d \leq 0.854$), third harmonic voltages can be completely eliminated, and sinusoidal phase currents are achieved. In overmodulation region ($0.854 \leq d \leq 1$), although the sinusoidal phase currents are unavailable, the third harmonic currents are reduced as much as possible. Moreover, in order to reduce CMV, two opposite large vectors are applied with equal dwell times to replace zero vectors in linear modulation region. Finally, the proposed FCS-MPC is investigated and compared with the conventional methods based on the experiments. The main contribution of this article is proposing an FCS-MPC method with improved dc-link utilization for five-phase PMSM drives. The dc-link utilization is improved by 17% compared with V3-based FCS-MPCs, and the superiorities of low CMV and low computation burden are kept.

The rest of this article is organized as follows. Section II presents the mathematical model of five-phase PMSM drives and CMV analysis. The conventional FCS-MPC methods are reviewed in Section III. The proposed method is illustrated and detailed in Section IV. The experimental results are presented and explained in Section V. Finally, Section VI concludes this article.

II. Five-Phase PMSMs and CMV Analysis

A. Mathematical Model of Five-Phase VSI and PMSM

The topology of a five-phase PMSM fed by a two-level voltage source inverter (VSI) is shown in Fig. 1.

The 32 (2^5) switching states generate 32 voltage vectors using the vector space decomposition method

$$\begin{bmatrix} u_\alpha \\ u_\beta \\ u_x \\ u_y \end{bmatrix} = \frac{2V_{\rm dc}}{5} \begin{bmatrix} 1 & \cos\delta & \cos 2\delta & \cos 3\delta & \cos 4\delta \\ 0 & \sin\delta & \sin 2\delta & \sin 3\delta & \sin 4\delta \\ 1 & \cos\delta & \cos 2\delta & \cos 3\delta & \cos 4\delta \\ 0 & \sin\delta & \sin 2\delta & \sin 3\delta & \sin 4\delta \end{bmatrix} \begin{bmatrix} S_{\rm a} \\ S_{\rm b} \\ S_{\rm c} \\ S_{\rm d} \\ S_{\rm e} \end{bmatrix} \tag{1}$$

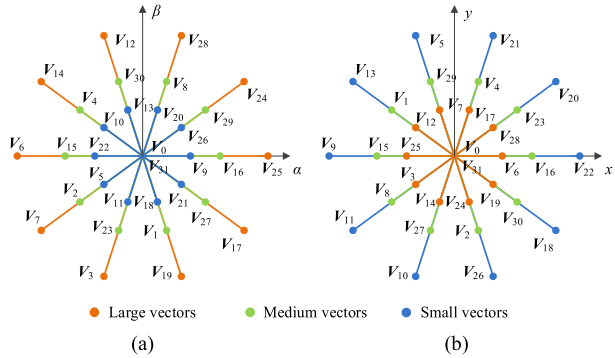

Fig. 2. Voltage vectors distribution of five-phase VSIs. (a) $\alpha\beta$ subspace. (b) xy subspace.

where $\delta = 2\pi/5$, $[S_{\rm a}, S_{\rm b}, S_{\rm c}, S_{\rm d}, S_{\rm e}]^{\rm T}$ represents the switching states, $[u_\alpha, u_\beta, u_x, u_y]^{\rm T}$ represents the voltages in $\alpha\beta$- and xy-subspaces.

The voltage vectors can be categorized into four groups according to the amplitudes in $\alpha\beta$ subspace, including large vectors ($0.6472V_{\rm dc}$), medium vectors ($0.4V_{\rm dc}$), small vectors ($0.2472V_{\rm dc}$), and zero vectors (0), as shown in Fig. 2.

The mathematical model of the surface-mounted five-phase PMSM in $\rm d_1q_1$ and $\rm d_3q_3$ frames can be expressed as

$$\begin{cases} u_{\rm d1} = R_{\rm s} i_{\rm d1} + \frac{d\psi_{\rm d1}}{dt} - \omega_{\rm e} L_{\rm s} i_{\rm q1} \\ u_{\rm q1} = R_{\rm s} i_{\rm q1} + \frac{d\psi_{\rm q1}}{dt} + \omega_{\rm e} L_{\rm s} i_{\rm d1} + \omega_{\rm e} \psi_{\rm m} \\ u_{\rm d3} = R_{\rm s} i_{\rm d3} + \frac{d\psi_{\rm d3}}{dt} - 3\omega_{\rm e} L_{\rm ls} i_{\rm q3} \\ u_{\rm q3} = R_{\rm s} i_{\rm q3} + \frac{d\psi_{\rm q3}}{dt} + 3\omega_{\rm e} L_{\rm ls} i_{\rm d3} \end{cases} \tag{2}$$

where $u_{\rm d1}$, $u_{\rm q1}$, $u_{\rm d3}$, and $u_{\rm q3}$ are the voltages, $i_{\rm d1}$, $i_{\rm q1}$, $i_{\rm d3}$ and $i_{\rm q3}$ are the currents in $\rm d_1q_1$ and $\rm d_3q_3$ reference frames, respectively. $R_{\rm s}$ represents the stator resistance, $L_{\rm s}$ represents the stator inductance, $L_{\rm ls}$ is the stator leakage inductance, $\psi_{\rm m}$ is the PM flux, $\omega_{\rm e}$ is the rotor speed.

Typically, for the surface-mounted five-phase PMSMs with distributed stator windings, the output torque can be expressed as

$$T_{\rm e} = 2.5 n_{\rm p} \psi_{\rm m} i_{\rm q1} \tag{3}$$

where $n_{\rm p}$ is pole pairs of the PMSM.

B. CMV Analysis in Five-Phase VSI

CMV is defined as the voltage between the neutral point of PMSM and the midpoint of dc-link

$$u_{\rm CM} = \frac{V_{\rm dc}}{5}(S_{\rm a} + S_{\rm b} + S_{\rm c} + S_{\rm d} + S_{\rm e}) - \frac{V_{\rm dc}}{2} \tag{4}$$

where $u_{\rm CM}$ represents the CMV.

It can be deduced that six different CMV values are generated, as given in Table I. It can be concluded as follows.

1) Zero vectors generate large CMV.
2) Medium vectors generate medium CMV.
3) Small and large vectors generate small CMV.

TABLE I
CMV GENERATED BY DIFFERENT VECTORS

	Voltage vectors					CMV
Zero vectors	V_0, V_{31}					$\pm 0.5V_{dc}$ large CMV
Large vectors	V_{25}	V_{24}	V_{28}	V_{12}	V_3	$\pm 0.1V_{dc}$
	V_6	V_7	V_{19}	V_{14}	V_{17}	Small CMV
Medium vectors	V_{16}	V_{29}	V_8	V_{30}	V_4	$\pm 0.3V_{dc}$
	V_{15}	V_2	V_{23}	V_1	V_{27}	Medium CMV
Small vectors	V_9	V_{26}	V_{20}	V_{13}	V_{10}	$\pm 0.1V_{dc}$
	V_{22}	V_5	V_{11}	V_{18}	V_{21}	Small CMV

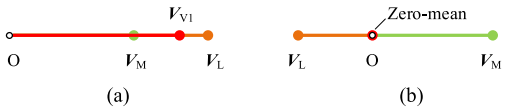

Fig. 3. Synthesis of V3 using aligned medium and large vectors. (a) $\alpha\beta$ subspace. (b) *xy* subspace.

III. EXISTING FCS-MPC METHODS

To reduce computation burden and improve steady-state performance in five-phase PMSM drives, the idea of V3 has been extensively studied. In this section, two latest FCS-MPC methods based on V3s are reviewed.

A. Conventional FCS-MPC With V3s

According to the distribution of voltage vectors, the aligned large and medium vectors in $\alpha\beta$ subspace have opposite directions in *xy* subspace. Taking advantage of this nature, the V3s are usually defined using the aligned large and medium vectors.

According to the volt-second balance, the amplitudes of V3s in $\alpha\beta$ and *xy* subspaces can be expressed as

$$\begin{cases} |\boldsymbol{V}_{\rm v}|_{\alpha\beta} = \lambda \cdot 0.6472V_{\rm dc} + (1-\lambda)\cdot 0.4V_{\rm dc} \\ |\boldsymbol{V}_{\rm v}|_{xy} = \lambda \cdot 0.2472V_{\rm dc} - (1-\lambda)\cdot 0.4V_{\rm dc} \end{cases} \tag{5}$$

where $|\boldsymbol{V}_{\rm v}|_{\alpha\beta}$ and $|\boldsymbol{V}_{\rm v}|_{xy}$ are the amplitudes of V3s in $\alpha\beta$ and *xy* subspaces, respectively. λ is the duty ratio of large vector.

Assuming that the *xy*-axes voltage is zero, yielding

$$\begin{cases} \lambda = 0.618 \\ |V_{\rm v}|_{\alpha\beta} = 0.5527V_{\rm dc}. \end{cases} \tag{6}$$

Hence, the *xy* axes voltages can be eliminated if the dwell times ratio for large vectors and medium vectors is fixed at 0.618:0.382, as shown in Fig. 3.

Generally, ten V3s are synthesized in total, as shown in Fig. 4. The amplitude of V3s is $0.5527V_{\rm dc}$, which is lower than large vectors ($0.6472V_{\rm dc}$).

Since the *xy*-voltage is inherently eliminated using V3s, the third harmonic terms are cancelled and prediction model can be simplified

$$\begin{cases} i_{\rm d1}^{k+1} = (1-\frac{R_{\rm s}T_{\rm s}}{L_{\rm s}})i_{\rm d1}^{k} + \omega_{\rm e}T_{\rm s}i_{\rm q1}^{k} + \frac{T_{\rm s}}{L_{\rm s}}u_{\rm d1}^{k} \\ i_{\rm q1}^{k+1} = (1-\frac{R_{\rm s}T_{\rm s}}{L_{\rm s}})i_{\rm q1}^{k} - \omega_{\rm e}T_{\rm s}i_{\rm d1}^{k} + \frac{T_{\rm s}}{L_{\rm s}}u_{\rm q1}^{k} - \omega_{\rm e}\frac{T_{\rm s}}{L_{\rm s}}\psi_{\rm m}. \end{cases} \tag{7}$$

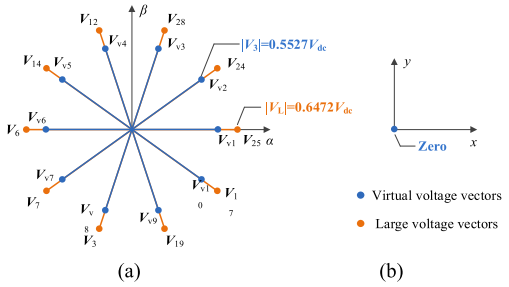

Fig. 4. Distribution of V3s in (a) $\alpha\beta$ subspace and (b) *xy* subspace.

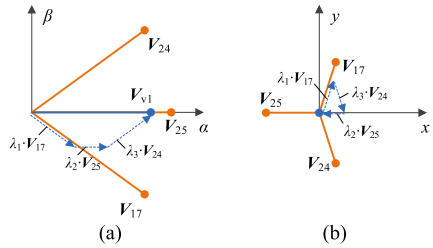

Fig. 5. Synthesis of V3 using three adjacent large vectors. (a) $\alpha\beta$ subspace. (b) *xy* subspace.

In order to compensate the one-step delay of FCS-MPC methods when implemented in digital controllers, the digital delay compensation is applied. The modified prediction model with delay compensation is expressed as

$$\begin{cases} i_{\rm d1}^{k+2} = (1-\frac{R_{\rm s}T_{\rm s}}{L_{\rm s}})i_{\rm d1}^{k+1} + \omega_{\rm e}T_{\rm s}i_{\rm q1}^{k+1} + \frac{T_{\rm s}}{L_{\rm s}}u_{\rm d1}^{k+1} \\ i_{\rm q1}^{k+2} = (1-\frac{R_{\rm s}T_{\rm s}}{L_{\rm s}})i_{\rm q1}^{k+1} - \omega_{\rm e}T_{\rm s}i_{\rm d1}^{k+1} + \frac{T_{\rm s}}{L_{\rm s}}u_{\rm q1}^{k+1} \\ \qquad -\omega_{\rm e}\frac{T_{\rm s}}{L_{\rm s}}\psi_{\rm m}. \end{cases} \tag{8}$$

Then, a cost function is defined as the two norm of $\rm d_1q_1$-axes current errors

$$G = \left|i_{\rm d1}^{*} - i_{\rm d1}^{k+2}\right|^2 + \left|i_{\rm q1}^{*} - i_{\rm q1}^{k+2}\right|^2. \tag{9}$$

Since the *xy*-axes voltage is eliminated with the definition of V3s, the harmonic terms are also removed from cost function. The vector that minimizes the cost function is selected and applied during the next sampling interval. The number of synthesized V3s is significantly reduced, which can reduce the computation burden. Nevertheless, zero vectors and medium vectors are available, medium and large CMV will be generated, which is harmful to the motor bearings.

B. Conventional CMV-Reduced FCS-MPC With V3s

To further improve the performance of V3-based FCS-MPC and reduce CMV in five-phase PMSM drives, a new definition of V3s is proposed recently [30].

Three adjacent large vectors are used to synthesize V3s, as shown in Fig. 5, where $\boldsymbol{V}_{\rm v1}$ is taken as an example for illustration.

Following the combination rule, the amplitudes of V3s in $\alpha\beta$ and *xy* subspaces can be expressed

$$\begin{cases} |\boldsymbol{V}_{\rm v}|_{\alpha\beta} = (\lambda_1 \cdot \cos(\frac{\pi}{5}) + \lambda_2 + \lambda_3 \cdot \cos(\frac{\pi}{5}))\cdot 0.6472V_{\rm dc} \\ |\boldsymbol{V}_{\rm v}|_{xy} = (\lambda_1 \cdot \cos(\frac{2\pi}{5}) - \lambda_2 + \lambda_3 \cdot \cos(\frac{2\pi}{5}))\cdot 0.2472V_{\rm dc} \end{cases} \tag{10}$$

where λ_1, λ_2, and λ_3 are the duty ratios of $\boldsymbol{V}_{17}$, $\boldsymbol{V}_{25}$ and $\boldsymbol{V}_{24}$, respectively.

Assuming $|\boldsymbol{V}_{\rm v}|_{xy} = 0$, and considering the condition that $\lambda_1+\lambda_2+\lambda_3 = 1$, yields

$$\begin{cases} \lambda_1 = 0.382 \\ \lambda_2 = 0.236 \\ \lambda_3 = 0.382 \\ |V_{\rm v}|_{\alpha\beta} = 0.5527V_{\rm dc}. \end{cases} \tag{11}$$

It is obvious that the V3s synthesized by adjacent large vectors have the same amplitude and distribution as that using medium and large vectors. Then, the resultant V3s are used to predict the currents evolution, and the one that minimizes the cost function is selected and applied during the next sampling interval. Since zero vectors and medium vectors that generate large and medium CMV are abandoned, CMV is effectively reduced.

However, although the computation burden is reduced and steady-state performance is improved in these V3-based FCS-MPC methods, the dc-link utilization is reduced due to the lower amplitude of V3s.

IV. Proposed FCS-MPC Methods

Since the V3s have lower amplitude, the maximum output voltage is limited, and the dc-link utilization is reduced in V3-based FCS-MPC methods. To address this issue, an FCS-MPC method with improved dc-link utilization is proposed in this section.

A. Vector Selection and Duty Ratio Estimation

Considering that zero and medium vectors generate large and medium CMV, which is not beneficial to CMV reduction, they are eliminated from the control set. Besides, small vectors generate small CMV, but the amplitude is much smaller, which will reduce the dc-link utilization. Therefore, only large vectors are selected as the candidates to carry out the optimization procedure. The harmonic currents in *xy* subspace are neglected in this step and the large vector that minimizes the cost function in (9) is selected.

Usually, it is not necessary to apply the selected large vector for the entire sampling interval. If the large vector is applied for the entire sampling interval, undesired current total harmonic distortion (THD) and torque ripples will be generated. Therefore, the duty ratio solution is adopted, which estimates the optimal dwell time during each sampling interval.

Assuming that the selected large vector is applied for $dT_{\rm s}$, where d is defined as duty ratio of the optimal vector. Then, the prediction model is modified with d

$$\begin{cases} i_{\rm d1}^{k+2} = (1-\frac{R_{\rm s}T_{\rm s}}{L_{\rm s}})i_{\rm d1}^{k+1} + \omega_{\rm e}T_{\rm s}i_{\rm q1}^{k+1} + d\frac{T_{\rm s}}{L_{\rm s}}u_{\rm d1}^{k+1} \\ i_{\rm q1}^{k+2} = (1-\frac{R_{\rm s}T_{\rm s}}{L_{\rm s}})i_{\rm q1}^{k+1} - \omega_{\rm e}T_{\rm s}i_{\rm d1}^{k+1} + d\frac{T_{\rm s}}{L_{\rm s}}u_{\rm q1}^{k+1} - \omega_{\rm e}\frac{T_{\rm s}}{L_{\rm s}}\psi_{\rm m}. \end{cases} \tag{12}$$

The duty ratio is determined such that the current errors are minimized. In other words, d is estimated to minimize the cost function, yielding

$$\frac{\partial G}{\partial d} = 0. \tag{13}$$

Applying (9) and (12) to (13), d can be calculated as

$$d = \frac{h_1 \cdot u_{\rm d1}^{k+1} + h_2 \cdot u_{\rm q1}^{k+1}}{\left(u_{\rm d1}^{\rm k+1}\right)^2 + \left(u_{\rm q1}^{\rm k+1}\right)^2} \tag{14}$$

where

$$\begin{aligned} h_1 &= \frac{L_{\rm s}}{T_{\rm s}}\left(i_{\rm d1}^{*} - \left(1-\frac{RT_{\rm s}}{L_{\rm s}}i_{\rm d1}^{k+1}\right) - \omega_{\rm e}T_{\rm s}i_{\rm q1}^{k+1}\right) \\ h_2 &= \frac{L_{\rm s}}{T_{\rm s}}\left(i_{\rm q1}^{*} - \left(1-\frac{RT_{\rm s}}{L_{\rm s}}i_{\rm q1}^{k+1}\right) + \omega_{\rm e}T_{\rm s}i_{\rm d1}^{k+1} + \frac{\omega_{\rm e}T_{\rm s}}{L_{\rm s}}\psi_{\rm m}\right). \end{aligned} \tag{15}$$

The duty ratio should be limited within the range $0 \le d \le 1$. So, the selected large vector is applied for $dT_{\rm s}$, and zero vector is applied for the remaining part of each sampling interval. It should be noticed that the maximum available output voltage is $0.6472V_{\rm dc}$ ($d = 1$), which is improved by 17% compared with the V3-based FCS-MPC methods.

B. Duty Ratio Reassignment

Although the dc-link utilization is improved using large vectors, large *xy*-axes voltages are generated, which will increase the current distortion and deteriorate the steady-state performance. To reduce the third harmonic currents, three adjacent large vectors are used to replace the selected large vector, and the duty ratios are reassigned. $\boldsymbol{V_{25}}$ is assumed as the optimal vector for illustration.

The combination of three adjacent large vectors $\boldsymbol{V_{17}}$, $\boldsymbol{V_{25}}$, and $\boldsymbol{V_{24}}$ can generate zero-mean *xy*-axes voltage component with specific dwell times [30]. Taking advantage of this nature, the duty ratios are reassigned based on the volt-second balance

$$\begin{cases} d = d_1\cos(\frac{\pi}{5}) + d_2 + d_3\cos(\frac{\pi}{5}) \\ d_0 = 1-(d_1+d_2+d_3) \end{cases} \tag{16}$$

where d_1, d_2, and d_3 are the reassigned duty ratios of $\boldsymbol{V_{17}}$, $\boldsymbol{V_{25}}$, and $\boldsymbol{V_{24}}$, respectively, and d_0 is the duty ratio of zero vector, which will be replaced by opposite large vectors to reduce CMV in the following step.

According to (11), if the duty ratios satisfy d_1:d_2:d_3 = 0.382:0.236:0.382, the *xy*-axes voltages can be eliminated completely. Applying (11) and the limitation $d_i \ge 0$ (i = 0, 1, 2 and 3) to (16), yielding

$$\begin{cases} d_1 = 0.4473d \\ d_2 = 0.2763d \\ d_3 = 0.4473d \\ d_0 = 1-d_1-d_2-d_3 \end{cases}, 0 < d \le 0.854. \tag{17}$$

Hence, the *xy*-axes voltages can be completely eliminated when d is within the range $0 \le d \le 0.854$ (linear modulation region). The equation d_1:d_2:d_3 = 0.382:0.236:0.382 cannot be satisfied if d is larger than 0.854 (overmodulation region). In other words, third harmonic currents will be generated and sinusoidal phase currents are not available when d>0.854. Therefore, (17) can only be adopted in linear modulation region, and further analysis is required for overmodulation region.

Although the *xy*-axes voltages cannot be completely eliminated in overmodulation region, it is possible to suppress the

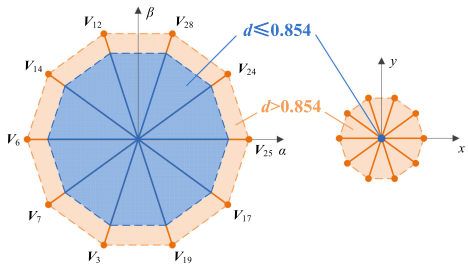

Fig. 6. Modulation region of the two modes.

harmonic components to some extent. It can be observed from Fig. 2 that $\boldsymbol{V_{17}}$ and $\boldsymbol{V_{24}}$ have opposite effects on *xy*-axes voltages compared with $\boldsymbol{V_{25}}$. Therefore, to reduce the *xy*-axes voltage as much as possible, $\boldsymbol{V_{17}}$ and $\boldsymbol{V_{24}}$ should be applied as long as possible. Thus, d_0 is set to 0. Moreover, in order to keep the volt-second balance, the dwell times of $\boldsymbol{V_{17}}$ and $\boldsymbol{V_{24}}$ should be equal, yielding

$$\begin{cases} d = d_1\cos(\frac{\pi}{5}) + d_2 + d_3\cos(\frac{\pi}{5}) \\ 1 = d_1 + d_2 + d_3 \\ d_1 = d_3. \end{cases} \tag{18}$$

Then, the reassigned duty ratios in overmodulation region can be obtained

$$\begin{cases} d_1 = 2.618(1-d) \\ d_2 = 5.236d - 4.236 \\ d_3 = 2.618(1-d) \\ d_0 = 0. \end{cases}, 0.854 < d \le 1 \tag{19}$$

In linear modulation region where $0 \le d \le 0.854$ (the blue area in Fig. 6), *xy*-axes voltages are eliminated and sinusoidal phase currents can be achieved. In overmodulation region where $0.854 \le d \le 1$ (the orange area in Fig. 6), *xy*-axes voltages cannot be completely eliminated, and the duty ratios are re-assigned to reduce the *xy*-axes voltages as much as possible. Although the sinusoidal phase currents are unavailable and third harmonic currents are inevitably generated in overmodulation region, the fundamental currents are well controlled, and torque performance will not be affected.

In reality, d is not constant and fluctuates within a narrow range. To avoid the frequent commutations between the two modes shown in (17) and (19), a comparator is designed to control the duty ratio reassignments.

In steady state, the transient terms in the voltage equation are neglected, and the amplitude of expected stator voltage can be estimated as

$$u_{\mathrm{s}} = \sqrt{\left(R_{\mathrm{s}} i_{\mathrm{d1}}^{*} - \omega_{\mathrm{e}}^{*} L_{\mathrm{s}} i_{\mathrm{q1}}^{*}\right)^2 + \left(R_{\mathrm{s}} i_{\mathrm{q1}}^{*} + \omega_{\mathrm{e}}^{*} L_{\mathrm{s}} i_{\mathrm{d1}}^{*} + \omega_{\mathrm{e}}^{*} \psi_{\mathrm{m}}\right)^2}. \tag{20}$$

On the other hand, the maximum phase voltage is generated when the five-phase VSI operates in ten-step mode, which can be calculated as

$$u_{\mathrm{max\_}L} = \frac{2}{\pi} V_{\mathrm{dc}} \tag{21}$$

where $u_{\mathrm{max\cdot L}}$ is the maximum phase voltage using large vectors.

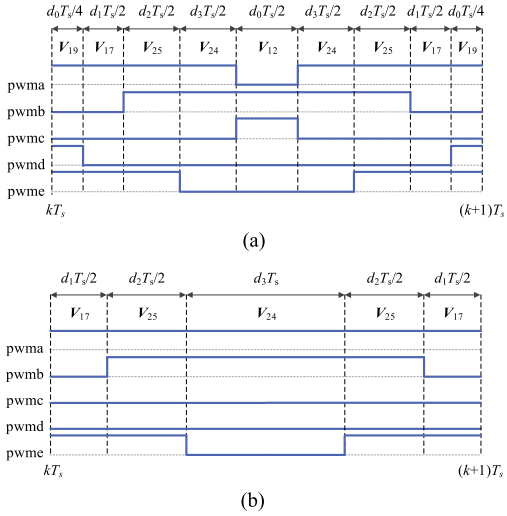

Fig. 7. Switching sequences of the proposed method in different regions. (a) $0 < d \le 0.854$. (b) $0.854 < d \le 1$.

Thus, the theoretical maximum phase voltage in linear modulation region can be expressed as

$$u_{\max} = 0.854 u_{\max\_L} = 0.5437 V_{\mathrm{dc}}. \tag{22}$$

The threshold of the comparator is fixed at $u_{\max}$. If the expected voltage is lower than $u_{\max}$, d is limited within the range $0 \le d \le 0.854$, which can reduce the third harmonic currents and achieve sinusoidal phase currents. The proposed duty ratio reassignments can be expressed as

$$\begin{cases} u_{\mathrm{s}} \le u_{\max} \Rightarrow \begin{cases} d \le 0.854 \Rightarrow \begin{cases} d_1 = 0.4473d \\ d_2 = 0.2763d \\ d_3 = 0.4473d \\ d_0 = 1 - d_1 - d_2 - d_3 \end{cases} \\ d > 0.854 \Rightarrow \begin{cases} d_1 = 0.382 \\ d_2 = 0.236 \\ d_3 = 0.382 \\ d_0 = 0 \end{cases} \end{cases} \\ u_{\mathrm{s}} \ge u_{\max} \Rightarrow \begin{cases} d \le 0.854 \Rightarrow \begin{cases} d_1 = 0.4473d \\ d_2 = 0.2763d \\ d_3 = 0.4473d \\ d_0 = 1 - d_1 - d_2 - d_3 \end{cases} \\ d > 0.854 \Rightarrow \begin{cases} d_1 = 2.618(1-d) \\ d_2 = 5.236d - 4.236 \\ d_3 = 2.618(1-d) \\ d_0 = 0 \end{cases} \end{cases} \end{cases} \tag{23}$$

C. Switching Patterns Designation

In conventional FCS-MPC with duty ratio optimization, the zero vectors are applied for $d_0 T_{\mathrm{s}}$ to regulate the volt-second value. However, the zero vectors will generate large CMV, which is destructive to motor bearings. Thus, the two opposite large vectors are applied with equal dwell times to replace the zero vectors. To avoid additional switching actions, adjacent large vectors are selected. The switching sequences are shown

TABLE II
COMBINATIONS OF THE OPPOSITE LAREGE VECTORS

V_{opt}	Combinations	V_{opt}	Combinations
V_{25}	$0.25V_{19}+0.5V_{12}+0.25V_{19}$	V_6	$0.25V_{12}+0.5V_{19}+0.25V_{12}$
V_{24}	$0.25V_{17}+0.5V_{14}+0.25V_{17}$	V_7	$0.25V_{14}+0.5V_{17}+0.25V_{14}$
V_{28}	$0.25V_{25}+0.5V_6+0.25V_{25}$	V_3	$0.25V_6+0.5V_{25}+0.25V_6$
V_{12}	$0.25V_{24}+0.5V_7+0.25V_{24}$	V_{19}	$0.25V_7+0.5V_{24}+0.25V_7$
V_{14}	$0.25V_{28}+0.5V_3+0.25V_{28}$	V_{17}	$0.25V_3+0.5V_{28}+0.25V_3$

where V_{opt} is the optimal large vector.

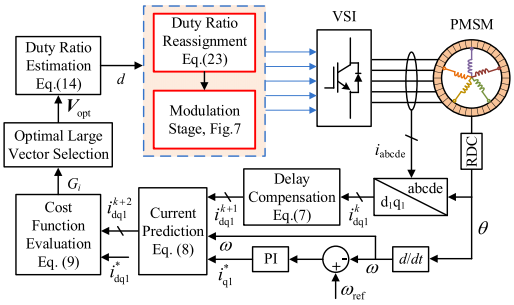

Fig. 8. Control block diagram of the proposed FCS-MPC.

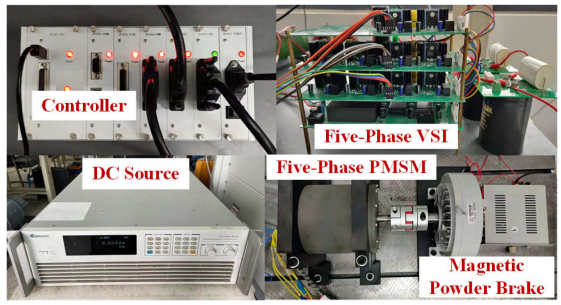

Fig. 9. Experimental platform of the five-phase PMSM.

TABLE III
PARAMETERS OF THE EXPERIMENTAL SYSTEM

Parameters	Values	Parameters	Values
DC-link voltage (V_{dc})	120V	Pole pairs (n_p)	4
Stator inductance (L_s)	6.5mH	Rated speed (ω_N)	1500rpm
Stator resistance (R_s)	0.3Ω	Rated current (I_N)	10A
PM flux linkage (ψ_m)	0.135Wb	Moment of inertia (J)	0.008kg·m^2

in Fig. 7, where V_{25} is assumed as the optimal vector for illustration.

The specific combinations of opposite large vectors are given in Table II.

D. Overall of Proposed FCS-MPC

The block diagram of proposed FCS-MPC is shown in Fig. 8. In the proposed FCS-MPC, phase currents are measured at the kth instant, i^k_{d1} and i^k_{q1} are acquired by applying coordinate transformation, and i^{k+1}_{d1} and i^{k+1}_{q1} are estimated to compensate the one-step delay. Then, the ten large vectors are applied to predict the currents evolution, and the one that minimizes the cost function is selected. The duty ratio is also estimated to reduce the tracking errors of d_1q_1-axes currents, which determine the electromechanical energy conversion.

To reduce the xy-axes voltages that are responsible for third harmonic currents, three adjacent large vectors are used to replace the selected large vector, and the duty ratios are reassigned, as expressed in (23). In linear modulation region ($0 < d \leq 0.854$), the xy-axes voltages are cancelled, and the third harmonic currents can be eliminated. In overmodulation region ($0.854 < d \leq 1$), although the xy-axes voltage cannot be completely eliminated, the volt-second balance in the $\alpha\beta$ subspace is kept and the xy-axes voltages are reduced as much as possible. Hence, the torque performance will not be affected.

Moreover, two opposite large vectors are applied with equal dwell times to replace zero vectors in linear modulation region, and the switching patterns are designed, which can effectively reduce CMV.

V. EXPERIMENTAL RESULTS

An experimental platform of five-phase PMSM has been set up to verify the proposed method, as shown in Fig. 9. A Chroma programmable dc source is used as the power supply. A Tamagawa resolver and a resolver to digital converter AD2S1210 are used to acquire the rotor position and speed. A TI DSP TMS320F28335 is used to implement the control methods with 10 kHz sampling frequency. The parameters of the experimental system are given in Table III.

The conventional FCS-MPC method with V3s reviewed in Section III-A is named as FCS-MPC-V3, and the CMV-reduced FCS-MPC reviewed in Section III-B is named as FCS-MPC-RCMV. For fair comparison, the duty ratio optimization is also applied to FCS-MPC-V3 and FCS-MPC-RCMV.

A. Comparison of DC-Link Utilization

According to the mathematical model of the five-phase PMSM, the stator voltage is positively associated with rotor speed in steady state. In other words, for a given dc-link voltage, the control method with higher dc-link utilization can realize higher maximum rotor speed.

The speed limitation comparison for a given dc-link voltage is shown in Fig. 10. In the comparison, the reference speed is set as 1500 rpm, which cannot be reached for the given dc-link voltage (120 V), to test the speed limitation of the studied methods. It is clear that the maximum speed of conventional FCS-MPC-V3 and FCS-MPC-RCMV is about 1200 r/min, while that of the proposed FCS-MPC is 1400 r/min. Thus, the proposed method can extend the speed range for a given dc-link voltage.

The experimental results of maximum phase voltage are shown in Fig. 11. According to the fast Fourier transform (FFT) analysis, the peak values of fundamental phase voltage are 64.4 and 64.3 V in FCS-MPC-V3 and FCS-MPC-RCMV, and 75.5V in proposed FCS-MPC, respectively. The dc-link utilization using the proposed FCS-MPC method is improved by about 17% compared with FCS-MPC-V3 and FCS-MPC-RCMV, which is identical to the theoretical analysis.

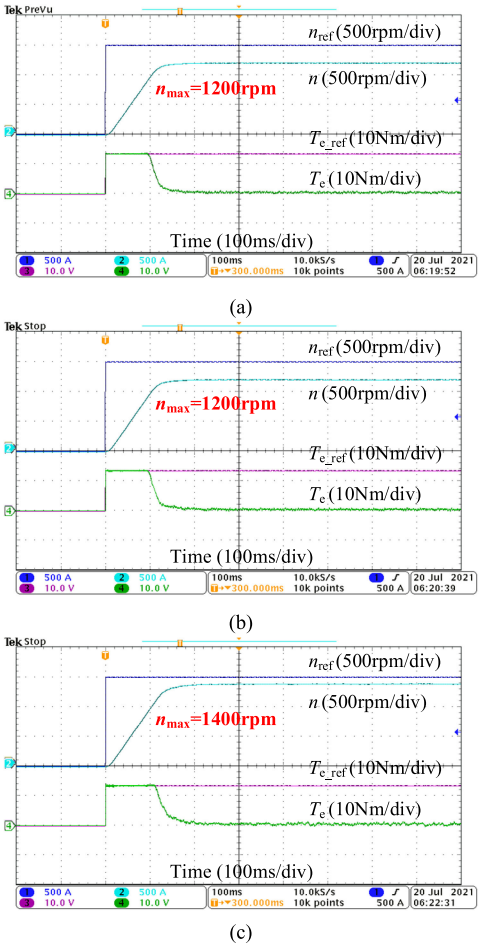

Fig. 10. Comparison of speed limitation. (a) FCS-MPC-V3. (b) FCS-MPC-RCMV. (c) Proposed FCS-MPC.

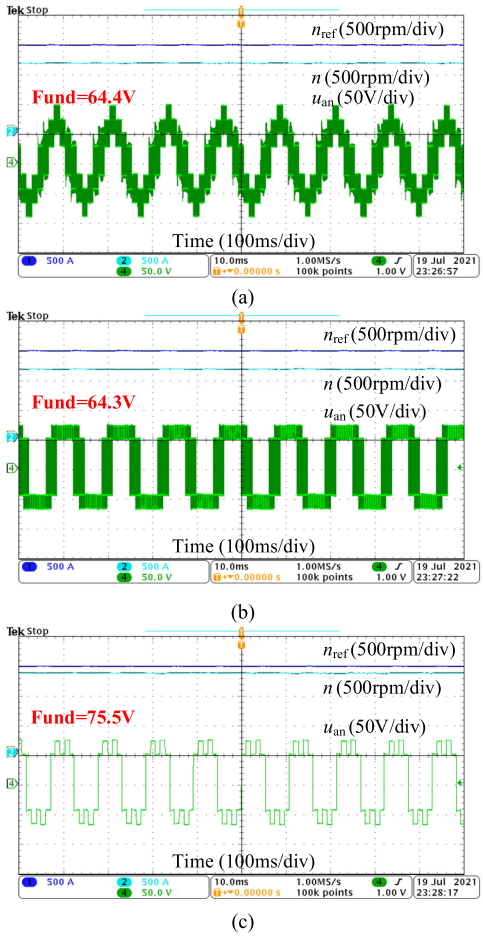

Fig. 11. Comparison of maximum phase voltage. (a) FCS-MPC-V3. (b) FCS-MPC-RCMV. (c) Proposed FCS-MPC.

TABLE IV
MAXIMUM SPEED AND VOLTAGE OF THE STUDIED METHODS

	FCS-MPC-V3	FCS-MPC-RCMV	Proposed FCS-MPC
Maximum Speed	1200rpm	1200rpm	1400rpm
Phase Voltage	64.4V	64.3V	75.5V

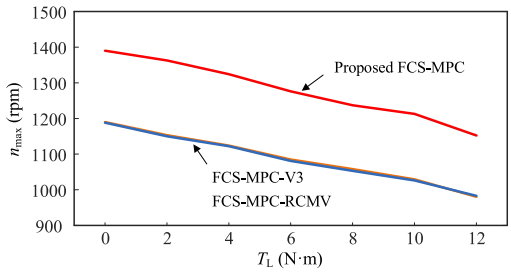

Fig. 12. Comparison of maximum speed under different load torques.

The maximum speed and peak phase voltage using the studied methods for the given dc-link voltage (120 V) are given in Table IV.

Moreover, the maximum speeds of the studied methods with different load torques are investigated, as shown in Fig. 12. It is obvious that, the proposed FCS-MPC can extend the speed range for given dc-link voltage.

B. Steady-State Performance

The steady-state performances are investigated with 10N·m load torque. Three different cases are considered as follows.

1) 600 r/min, where d is smaller than 0.854.
2) 1000 r/min, where d is close to 0.854.
3) 1100 r/min, where d is larger than 0.854.

The experimental results of phase currents, torque and CMV at 600 and 1000 r/min are shown in Figs. 13 and 14, respectively. It can be found that the CMV using conventional FCS-MPC-V3 is the largest ($\pm 0.5V_{dc}$), due to the absence of CMV reduction. CMV is mitigated to $\pm 0.1V_{dc}$ in the proposed FCS-MPC, reduced by 80% compared with FCS-MPC-V3. The THD of phase currents are obtained according to the FFT analysis, which indicates that the three studied methods have similar currents distortion in linear modulation region.

Fig. 15 shows the experimental results of the proposed method at 1100 r/min. Since the maximum speed of FCS-MPC-V3 and FCS-MPC-RCMV is about 1020 r/min, the experimental results at 1100 r/min are absent. In overmodulation region, the xy-axes

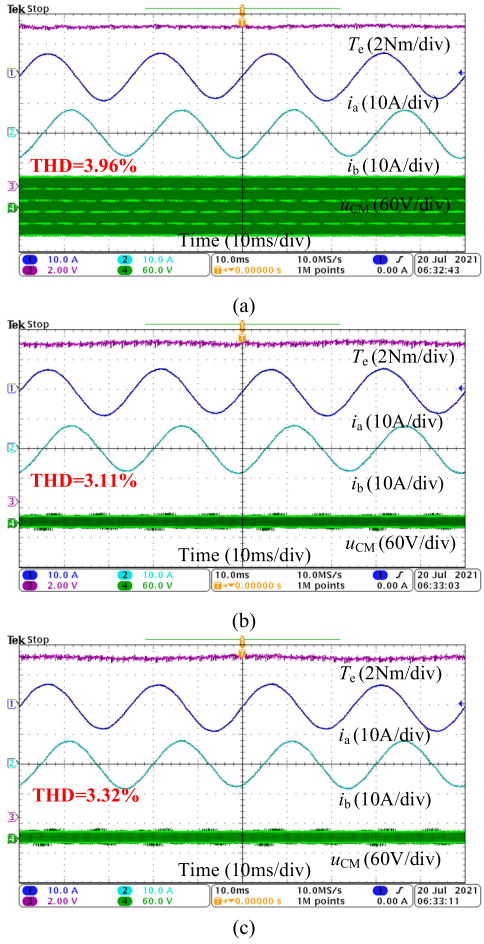

Fig. 13. Experimental results of phase currents, torque and CMV at 600 r/min. (a) FCS-MPC-V3. (b) FCS-MPC-RCMV. (c) Proposed FCS-MPC.

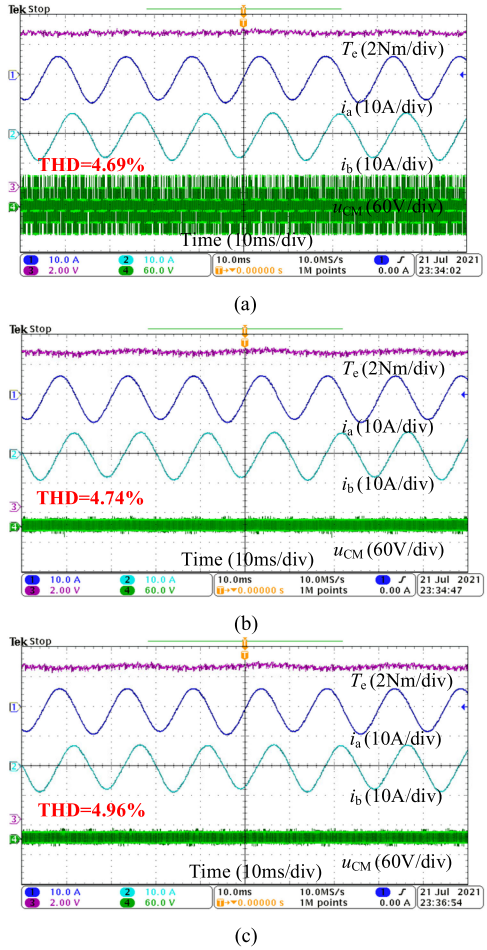

Fig. 14. Experimental results of phase currents, torque and CMV at 1000 r/min. (a) FCS-MPC-V3. (b) FCS-MPC-RCMV. (c) Proposed FCS-MPC.

voltages cannot be completely eliminated, and sinusoidal phase currents are unavailable. Although the current THD is inevitably increased due to third harmonic currents, the d_1q_1-axes currents are well controlled. As a result, the torque ripples are kept similar to that in linear modulation region.

Moreover, the current THD, torque ripples and switching frequency at different speeds are compared, as shown in Fig. 16. The current THD values are obtained according to the FFT analysis.

The torque ripples are calculated as

$$T_r = \sqrt{\frac{1}{n}\sum_{i=1}^{n}(T_{\text{ave}} - T_i)^2} \tag{24}$$

where T_{ave} is the average torque, T_i is actual value of the torque data, and n is the data points.

The average switching frequency is defined as

$$f_{\text{sw}} = \frac{1}{5T_w}\sum_{k=\text{a}}^{e} N_k \tag{25}$$

where T_w is the time window in which the ON-OFF times of IGBTs are counted, and T_w is set as 0.2s in this test. N_k represents the ON-OFF times of leg k (k = a, b, c, d, e).

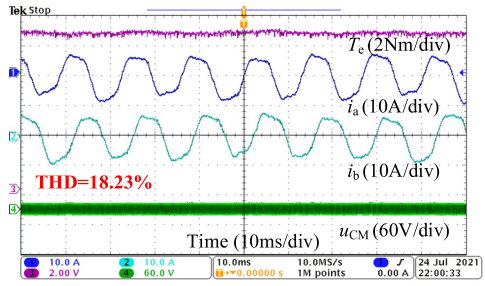

Fig. 15. Experimental results of phase currents, torque and CMV using proposed FCS-MPC at 1100 r/min.

It can be observed that the current THD of the proposed method is similar to that of FCS-MPC-V3 and FCS-MPC-RCMV in linear modulation region. The torque ripples of the proposed method are similar to that of the FCS-MPC-RCMV, and larger than the conventional FCS-MPC-V3, which is the price paid for CMV reduction [31]. In overmodulation region, although the current THD of the proposed method is increased due to third harmonic currents, the torque ripples are not affected.

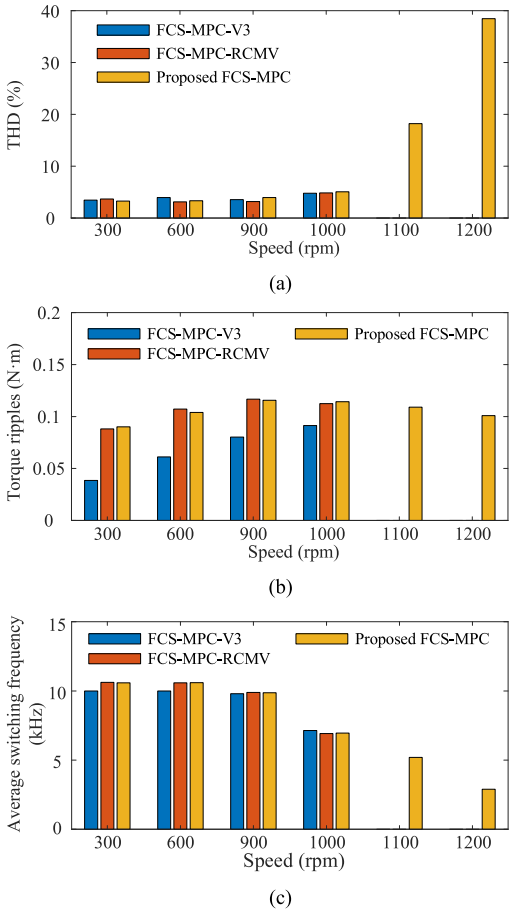

Fig. 16. Comparisons of (a) current THD, (b) torque ripples, and (c) average switching frequency.

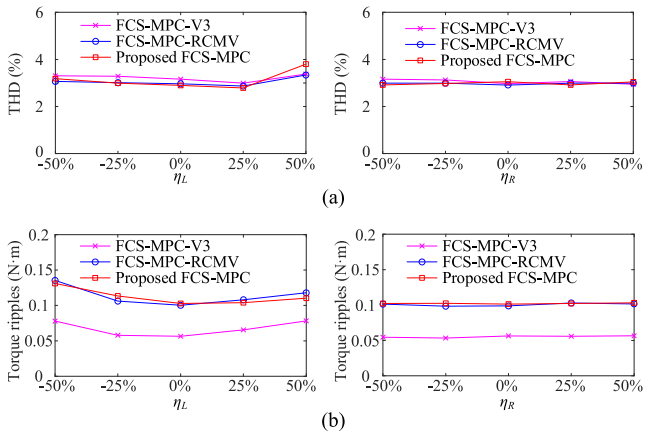

Fig. 17. THD and torque ripples of the studied methods at 600 r/min with different parameters mismatch. (a) Total harmonic distortions. (b) Torque ripples.

TABLE V
PERFORMANCE EVALUATION OF THE STUDIED METHODS

Performances	FCS-MPC-V3	FCS-MPC-RCMV	Proposed FCS-MPC
CMV reduction	$\pm 0.5V_{dc}$	$\pm 0.1V_{dc}$	$\pm 0.1V_{dc}$
Dc-link utilization	Low	Low	High
Speed range	Narrow	Narrow	Wide
Torque ripples	Smallest	Small	Small
Dynamic performance	Fast	Fast	Fast
Calculation time	30.3μs	30.5μs	31.8μs

Moreover, the switching frequency of the proposed method is similar to the conventional FCS-MPC-RCMV in linear modulation region. The switching frequencies of the proposed method and FCS-MPC-RCMV are slightly higher than of FCS-MPC-V3 due to the additional transitions between two adjacent sampling intervals, which is the cost of CMV reduction. In overmodulation region, the average switching frequency is reduced, as depicted in Fig. 16(c).

To analyze the parameter sensitivities of the proposed method, the parameter mismatch ratio η_x is defined

$$\eta_{\mathrm{x}} = \frac{X_{\mathrm{a}} - X_{\mathrm{r}}}{X_{\mathrm{r}}} \times 100\% \tag{26}$$

where X_{r} and X_{a} represent the rated and actual value of the stator resistance and inductance, respectively.

Fig. 17 compares the effects of parameter mismatches on the studied methods. It is clear that the stator resistance and inductance mismatches have negligible effects on current THD and torque ripples.

C. Dynamic Performance Comparison

The dynamic performances of the studied methods are investigated in two cases: the step-up and step-down changes of torque reference, as shown in Fig. 18. It is clear that the settling times of the studied methods are nearly the same. Therefore, fast dynamic performance is also kept in the proposed method.

D. Overall Comparison of Studied Methods

Finally, in order to evaluate the proposed FCS-MPC method clearly, the performances of the studied methods are given in Table V. The CMV is effectively mitigated using the proposed FCS-MPC, reduced by 80% compared with FCS-MPV-V3. The dc-link utilization is improved by about 17% compared with the conventional methods, as a result, the speed range is extended. In linear modulation region, satisfactory current THD and torque ripples are achieved using the proposed method. Although the current THD is increased in overmodulation region that FCS-MPC-V3 and FCS-MPC-RCMV cannot reach, the torque ripples are not increased. Moreover, the calculation time of the studied methods are compared, which indicates that the proposed method achieves similar computation burden compared with FCS-MPC-V3 and FCS-MPC-RCMV.

VI. CONCLUSION

This article proposes an FCS-MPC method with improved dc-link utilization for five-phase PMSM drives. In the proposed method, small and medium vectors are eliminated, and only ten

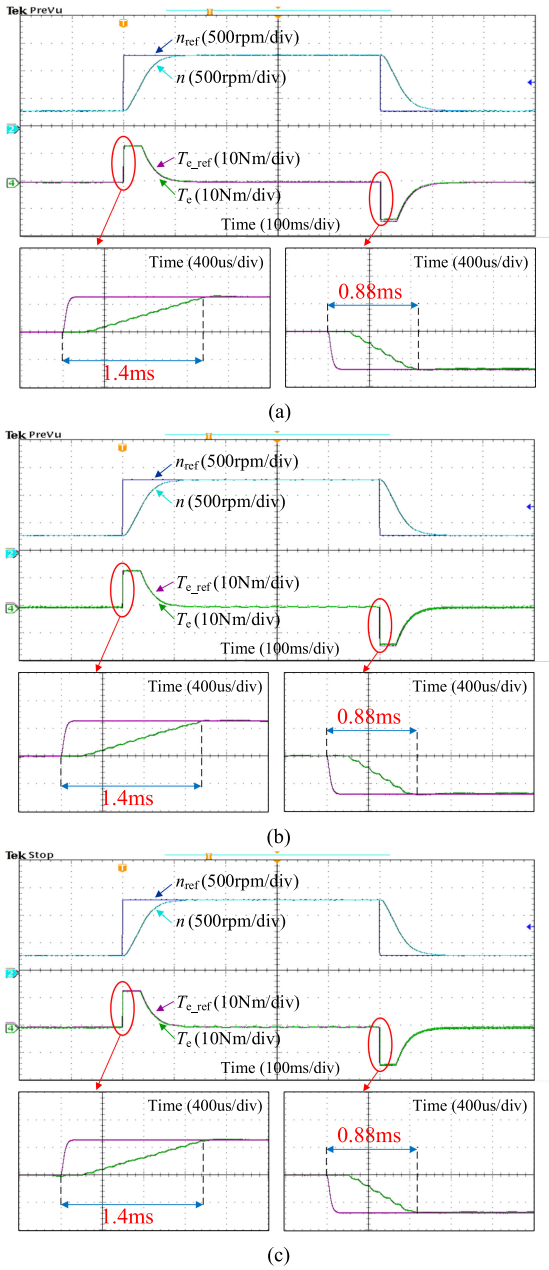

Fig. 18. Experimental results of dynamic response. (a) FCS-MPC-V3. (b) FCS-MPC-RCMV. (c) Proposed FCS-MPC.

large vectors are used to predict the currents evolution and evaluate the cost function. The third harmonic terms are cancelled from the cost function, and the large vector that minimizes the simplified cost function is selected. Then, the duty ratio of the selected vector is also estimated, which can reduce the current tracking errors. In order to control the third harmonic currents, three adjacent large vectors are used to replace the optimal vector based on volt-second balance, and the duty ratios are reassigned. Finally, two opposite large vectors are applied with equal dwell times to replace zero vectors in linear modulation region, which can effectively reduce CMV. The feasibilities of the proposed method are validated by experimental results. For clarity, the salient superiorities of the proposed method are summarized as follows.

1) CMV is mitigated to $\pm 0.1 V_{\rm dc}$, reduced by 80% compared with FCS-MPC-V3.
2) DC-link utilization is improved by 17%, and the speed range is extended.
3) Superior steady-state performance is achieved, torque ripples are well controlled at different speeds.
4) The computation burden is similar to that of conventional V3-based FCS-MPC methods.

REFERENCES

[1] Y. Luo and C. Liu, "Pre- and post-fault tolerant operation of a six-phase PMSM motor using FCS-MPC without controller reconfiguration," *IEEE Trans. Veh. Technol.*, vol. 68, no. 1, pp. 254–263, Jan. 2019.
[2] B. Tian, L. Sun, M. Molinas, and Q. An, "Repetitive control based phase voltage modulation amendment for FOC-based five-phase PMSMs under single-phase open fault," *IEEE Trans. Ind. Electron.*, vol. 68, no. 3, pp. 1949–1960, Mar. 2021.
[3] Q. Chen, L. Gu, Z. Lin, and G. Liu, "Extension of space-vector-signal-injection-based MTPA control into SVPWM fault-tolerant operation for five-phase IPMSM," *IEEE Trans. Ind. Electron.*, vol. 67, no. 9, pp. 7321–7333, Sep. 2020.
[4] T. Tao, W. Zhao, Y. He, Y. Cheng, S. Saeed, and J. Zhu, "Enhanced fault-tolerant model predictive current control for a five-phase PM motor with continued modulation," *IEEE Trans. Power Electron.*, vol. 36, no. 3, pp. 3236–3246, Mar. 2021.
[5] T. Tao, W. Zhao, Y. Du, Y. Cheng, and J. Zhu, "Simplified fault-tolerant model predictive control for a five-phase permanent-magnet motor with reduced computation burden," *IEEE Trans. Power Electron.*, vol. 35, no. 4, pp. 3850–3858, Apr. 2020.
[6] Y. Sui, P. Zheng, Z. Yin, M. Wang, and C. Wang, "Open-circuit fault-tolerant control of five-phase PM machine based on reconfiguring maximum round magnetomotive force," *IEEE Trans. Ind. Electron.*, vol. 66, no. 1, pp. 48–59, Jan. 2019.
[7] F. Bu, T. Pu, Q. Liu, B. Ma, M. Degano, and C. Gerada, "Four-degree-of-freedom overmodulation strategy for five-phase space vector pulse width modulation," *IEEE J. Emerg. Sel. Topics Power Electron.*, vol. 9, no. 2, pp. 1578–1590, Apr. 2021.
[8] L. Vancini, M. Mengoni, G. Sala, G. Rizzoli, L. Zarri, and A. Tani, "A trigonometric solution to the problem of overmodulation in five-phase inverters," in *Proc. IEEE Energy Convers. Congr. Expo.*, 2020, pp. 5416–5542.
[9] A. G. Yepes, J. Doval-Gandoy, and H. A. Toliyat, "Improvement in dc-link utilization with reduced current and torque deterioration for five-phase drives by combination of circulating-current filters and simple carrier-based PWM based on closed-form expressions," *IEEE Trans. Ind. Electron.*, vol. 68, no. 2, pp. 960–971, Feb. 2021.
[10] M. J. Durán, J. Prieto, and F. Barrero, "Space vector PWM with reduced common-mode voltage for five-phase induction motor drives operating in overmodulation zone," *IEEE Trans. Power Electron.*, vol. 28, no. 8, pp. 4030–4040, Aug. 2013.
[11] J. Prieto, F. Barrero, M. J. Duran, S. Toral Marin, and M. A. Perales, "SVM procedure for *n*-phase VSI with low harmonic distortion in the overmodulation region," *IEEE Trans. Ind. Electron.*, vol. 61, no. 1, pp. 92–97, Jan. 2014.
[12] S. Liu and C. Liu, "Virtual-vector-based robust predictive current control for dual three-phase PMSM," *IEEE Trans. Ind. Electron.*, vol. 68, no. 3, pp. 2048–2058, Mar. 2021.
[13] L. Vancini, M. Mengoni, G. Rizzoli, G. Sala, L. Zarri, and A. Tani, "Carrier-based PWM overmodulation strategies for five-phase inverters," *IEEE Trans. Power Electron.*, vol. 36, no. 6, pp. 6988–6999, Jun. 2021.
[14] A. G. Yepes and J. Doval-Gandoy, "Overmodulation method with adaptive *x-y* current limitation for five-phase induction motor drives," *IEEE Trans. Ind. Electron.*, to be published, doi: 10.1109/TIE.2021.3068687.
[15] A. G. Yepes and J. Doval-Gandoy, "Simple carrier-based PWM for prolonged high dc-link utilization for symmetrical and asymmetrical *n*-phase AC drives," *IEEE Trans. Power Electron.*, vol. 36, no. 8, pp. 8696–8712, Feb. 2021.
[16] W. Huang, W. Hua, F. Chen, M. Hu, and J. Zhu, "Model predictive torque control with SVM for five-phase PMSM under open-circuit fault condition," *IEEE Trans. Power Electron.*, vol. 35, no. 5, pp. 5531–5540, May 2020.

[17] W. Hua, F. Chen, W. Huang, G. Zhang, W. Wang, and W. Xia, "Multi-vector-based model predictive control with geometric solution of a five-phase flux-switching permanent magnet motor," *IEEE Trans. Ind. Electron.*, vol. 67, no. 12, pp. 10035–10045, Dec. 2020.
[18] J. J. Aciego, I. G. Prieto, and M. J. Duran, "Model predictive control of six-phase induction motor drives using two virtual voltage vectors," *IEEE J. Emerg. Sel. Topics Power Electron.*, vol. 7, no. 1, pp. 321–330, Mar. 2019.
[19] W. Wang, Y. Fang, S. Chen, and Q. Zhang, "Finite control set model predictive current control of a five-phase PMSM with virtual voltage vectors and adaptive control set," *CES Trans. Elect. Mach. Syst.*, vol. 2, no. 1, pp. 136–141, Mar. 2018.
[20] A. B. howate, M. V. Aware, and S. Sharma, "Predictive torque control algorithm for a five-phase induction motor drive for reduced torque ripple with switching frequency control," *IEEE Trans. Power Electron.*, vol. 35, no. 7, pp. 7282–7294, Jul. 2020.
[21] W. Zhao, T. Tao, J. Zhu, H. Tan, and Y. Du, "A novel finite-control-set model predictive current control for five-phase PM motor with continued modulation," *IEEE Trans. Power Electron.*, vol. 35, no. 7, pp. 7261–7270, Jul. 2020.
[22] C. Xue, W. Song, X. Wu, and X. Feng, "A constant switching frequency finite-control-set predictive current control method of a five-phase inverter with duty-ratio optimization," *IEEE Trans. Power Electron.*, vol. 33, no. 4, pp. 3583–3594, Apr. 2018.
[23] Y. Luo and C. Liu, "Model predictive control for a six-phase PMSM motor with a reduced-dimension cost function," *IEEE Trans. Ind. Electron.*, vol. 67, no. 2, pp. 969–979, Feb. 2020.
[24] M. J. Duran, F. Barrero, and J. Prieto, "DC-bus utilization and over-modulation performance of five-phase voltage source inverters using model predictive control," in *Proc. IEEE Int. Conf. Ind. Technol.*, 2010, pp. 1501–1506.
[25] B. Yu, W. Song, J. Li, B. Li, and M. S. R. Saeed, "Improved finite control set model predictive current control for five-phase VSIs," *IEEE Trans. Power Electron.*, vol. 36, no. 6, pp. 7038–7048, Jun. 2021.
[26] A. Bhowate, M. V. Aware, and S. Sharma, "Predictive torque control of five-phase induction motor drive using successive cost-functions for CMV elimination," *IEEE Trans. Power Electron.*, vol. 36, no. 12, pp. 14133–14141, Dec. 2021.
[27] U. T. Shami and H. Akagi, "Experimental discussions on a shaft end-to-end voltage appearing in an inverter-driven motor," *IEEE Trans. Power Electron.*, vol. 24, no. 6, pp. 1532–1540, Jun. 2009.
[28] M. J. Duran, J. Prieto, F. Barrero, J. A. Riveros, and H. Guzman, "Space-vector PWM with reduced common-mode voltage for five-phase induction motor drives," *IEEE Trans. Ind. Electron.*, vol. 60, no. 10, pp. 4159–4168, Oct. 2013.
[29] Z. Liu, P. Wang, W. Sun, Z. Shen, and D. Jiang, "Sawtooth carrier-based PWM methods with common-mode voltage reduction for symmetrical multiphase two-level inverters with odd phase number," *IEEE Trans. Power Electron.*, vol. 36, no. 1, pp. 1171–1183, Jan. 2021.
[30] B. Yu, W. Song, Y. Guo, J. Li, and M. S. R. Saeed, "Virtual voltage vector-based model predictive current control for five-phase VSIs with common-mode voltage reduction," *IEEE Trans. Transp. Electrific.*, vol. 7, no. 2, pp. 706–717, Jun. 2021.
[31] M. J. Durán, J. A. Riveros, and F. Barrero, "Reduction of common-mode voltage in five-phase induction motor drives using predictive control techniques," *IEEE Trans. Ind. Appl.*, vol. 48, no. 6, pp. 2059–2067, Nov./Dec. 2012.

Bin Yu (Student Member, IEEE) received the B.S. degree in electrical engineering in 2015 from Southwest Jiaotong University, Chengdu, China, where he is currently working toward the Ph.D. degree in electrical engineering.

His current research interests include power electronics and multiphase machine drives.

Wensheng Song (Member, IEEE) received the B.S. degree in electronic and information engineering and the Ph.D. degree in electrical engineering from Southwest Jiaotong University, Chengdu, China, in 2006 and 2011, respectively.

From September 2009 to September 2010, he was a Visiting Scholar with the Department of Electrical Engineering and Computer Science, University of California at Irvine, Irvine, CA, USA. From July 2015 to December 2015, he was a Visiting Scholar with the University of Alberta, Edmonton, AB, Canada. He is currently a Full Professor with the School of Electrical Engineering, Southwest Jiaotong University. His current research interests include digital control and modulation methods of electrical ac–dc–ac railway traction drive systems and multilevel converters.

Yongqi Guo received the B.S. degree in electrical engineering in 2019 from Southwest Jiaotong University, Chengdu, China, where he is currently working toward the M.S. degree in electrical engineering.

His current research interests include the power electronics and motor drives.

Mahmoud S. R. Saeed was born in Qena, Egypt, in 1991. He received the B.S. and the M.S. degrees in electrical power and machines engineering from the Faculty of Engineering, South Valley University, Qena, Egypt, in 2013 and 2018, respectively. He is currently working toward the Ph.D. degree from Southwest Jiaotong University, Chengdu, China.

Since 2015, he has been with the Department of Electrical Engineering, Faculty of Engineering, South Valley University, Qena, Egypt, first as an Administrator and a Research Assistant since 2018, and after that as an Assistant Lecturer. His research interests include electrical machines design and control, power electronics and drive systems, and renewable energy systems.